SUSPENDED NANOPARTICLES ON MIXED CONVECTION FLOW OF A JEFFREY FLUID DUE TO A HORIZONTAL CIRCULAR CYLINDER WITH VISCOUS DISSIPATION

by

Syazwani MOHD ZOKRI, Nur Syamilah ARIFIN, Abdul Rahman MOHD KASIM, and Mohd Zuki SALLEH*

Faculty of Industrial Sciences and Technology, University Malaysia Pahang, Pahang, Malaysia

Original scientific paper
https://doi.org/10.2298/TSCI181027106M

The non-Newtonian Jeffrey fluid model describes the viscoelastic property that elucidates the dual components of relaxation and retardation times. Nonetheless, there has been considerable attention on its unsatisfactory thermal performance. The model of nanofluid is contemporarily in the limelight due to its superior thermal performance compared to the conventional fluid. The proposed study herein aims to examine the Jeffrey nanofluid model over a horizontal circular cylinder with mixed convection flow. The flow analysis is performed based on the Buongiorno model with the integration of Brownian motion and thermophoresis diffusion parameters. The influence of frictional heat is also accounted. The non-dimensional and non-similarity transformation variables are utilized to reduce the dimensional governing equations into three non-dimensional PDE. Subsequently, the obtained PDE are tackled numerically through the Keller-box method. Certain continent parameters are investigated with regards to the identified distributions. A comparative study is executed based on previous studies, which indicates good agreement with results of the current study. The findings specify that the transition of boundary-layer from laminar to turbulent flows happens for dissimilar values of mixed convection parameter, Deborah number, Brownian motion and Eckert number. In particular, the boundary-layer separates from cylinder for positive (heated cylinder) and negative (cooled cylinder) values of mixed convection parameter. Heating the cylinder defers the separation of boundary-layer, while cooling the cylinder carries the separation point close to the lower stagnation point.

Key words: *Jeffrey fluid, suspended nanoparticles, horizontal circular cylinder, mixed convection, viscous dissipation*

Introduction

Heating or cooling techniques have been widely exploited in numerous fields inclusive of manufacturing, transportation, and production of thin-film solar energy collector devices. Nevertheless, it is relatively difficult for high-energy devices to achieve desired cooling rate by virtue of the unsatisfactory thermal performance of the conventional fluids. Latest methods like abrasion, clogging and additional pressure loss have been suggested to prevail the short coming, however, none of them demonstrates prolific outcome [1]. An engineered colloid known as nanofluid, being composed of the combination of solid-liquid particles was acclaimed to boost the thermal properties of the conventional fluid. It comprises of extremely

* Corresponding author, e-mail: zuki@ump.edu.my

small nanometer-sized particles called as nanoparticles that disseminated in the conventional fluids of low thermal conductivity. Some examples of nanoparticles include oxides (Al_2O_3, CuO, TiO_2, SiO_2), metals (Al, Cu), nitrides (AlN, SiN), carbides (SiC), or non-metals (graphite and carbon nanotubes), whereas organic liquids (tri-ethylene-glycols, ethylene, refrigerants, *etc.*), water, polymeric solution, bio-fluids, oil and lubricants, and other liquids are the conventional fluids. Nanofluid has also been experimentally corroborated by many in enhancing the thermal performance of the conventional fluids. This include the experiment conducted by Eastman *et al.* [2], whereby the thermal conductivity of water was upgraded to nearly 60% with the suspension of only 5% volume of CuO particles. In another study, Eastman *et al.* [3] discovered that the ethylene glycol containing copper nanoparticles have significantly improved the thermal conductivity in contrast to the ethylene glycol containing oxide particles. It is evident that with 0.3% volume of copper nanoparticles, the thermal performance of ethylene glycol has improved about 40%. Afterwards, Choi *et al.* [4] revealed that the dispersion of 1% volume of nanotubes has remarkably increased more than 2.5 thermal conductivity ratio of oil. The study was continued theoretically since then, including the flow analysis of the nanofluid model from the vertical plate and the stretching sheet by Kuznetsov and Nield [5] and Khan and Pop [6] on the respective vertical plate and the stretching sheet. The nanofluid model considered was the idea of Buongiorno that adapted the Brownian motion and thermophoresis diffusion parameters. Several attempts concerning this fluid model may also be found from the works [7-9] and many investigations in that.

Among the conventional fluids documented in the publications, the simple but elegant Jeffrey fluid model has been taken into account as a conventional fluid. This fluid model is categorized into the non-Newtonian fluid, where its rheological behavior is not anymore applicable to the Navier Stokes equation and its attributes are insufficient to be foreseen by a single relation. The manifestation of the two relaxation and retardation times effects in the Jeffrey fluid model is among the primary characteristic that differentiate it from the remaining fluids. This model also determines time derivatives as the substitutes for the convected derivatives. In particular, the Jeffrey nanofluid model from a convectively heated stretching sheet was attempted by Shehzad *et al.* [10]. They noticed that the increase of Biot number values led to the improvement of the temperature and nanoparticles concentration profiles. In another study, Dalir *et al.* [11] investigated the entropy generation effect for MHD flow of Jeffrey nanofluid over a stretching sheet. The entropy generation number was concluded to strongly vary due to the variation of the Lewis number and thermophoresis diffusion parameters. The impacts of double stratification and thermal radiation in the Jeffrey fluid with suspended nanoparticles on a stretching sheet were discussed by Abbasi *et al.* [12]. The reduction of temperature and nanoparticle concentration was observed following the elevation of the stratification of the thermal and nanoparticle concentrations. Recent development of this fluid model may be retrieved in the published studies by Hayat *et al.* [13] and Sharma and Gupta [14].

In respect to the flow analysis from a horizontal circular cylinder, Merkin [15] deliberated the mixed convection flow problem due to a viscous fluid. The boundary-layer separation was described comprehensively for the cases of cooled and heated cylinders over dissimilar values of mixed convection parameter. His study has revealed that the boundary-layer separation comes to be delayed when mixed convection parameter gets larger. Similar analysis was also discoursed by Nazar *et al.* [16] and Anwar *et al.* [17] in the respective micropolar and viscoelastic fluids. Their studies have exposed that the separation of boundary-layer flow hinges on the fluid under exploration. Considering the Newtonian heating condition in a viscous fluid, Salleh *et al.* [18] revealed that the escalation of mixed convection parameters has brought the separation point closer to the lower stagnation point, which found to be opposite to that of Merkin [15], Nazar *et al.* [16], and Anwar *et al.* [17]. Furthermore, the convectively heated nanofluid with porous medium was addressed by Rashad *et al.* [19], where the boundary-layer separation was concluded to encounter singularity at $x = 120°$. Following Rashad *et al.* [19], Tham *et al.* [20] directed their study on the constant wall temperature. They found that the boundary-layer separation was suppressed between $0° \leq x \leq 180°$, which is more than what was acquired by Rashad *et al.* [19].

It should be noted that majority of the studies highlighted the Jeffrey nanofluid model from the stretching sheet. On the other hand, investigation on the Jeffrey nanofluid from a horizontal circular cylinder has been scant. Thereupon, the current study focuses on the problem pertaining to suspended nanoparticles on mixed convection flow of a Jeffrey fluid passing over a horizontal circular cylinder with the viscous dissipation effect. Here, the presence of viscous dissipation cannot be overlooked particularly when dealing with highly viscous fluid or during rapid movement of the fluid. In fact, the convective heat transfer is predominantly being governed by the rheological behavior of fluid.

Problem formulation

According to Qasim [21], the constitutive equation for the model of Jeffrey fluid is:

$$\boldsymbol{\tau} = -p\mathbf{I} + \mathbf{S}, \quad \mathbf{S} = \frac{\mu}{1+\lambda}\left[\mathbf{R_1} + \lambda_1\left(\frac{\partial \mathbf{R_1}}{\partial t} + \vec{\mathbf{V}}\nabla\right)\mathbf{R_1}\right]$$

where $\boldsymbol{\tau}$, $\mathbf{I}$, $\mathbf{S}$, p, and μ are the Cauchy stress tensor, identity tensor, extra stress tensor, pressure, and dynamic viscosity, respectively. Furthermore, the material parameters of the Jeffrey fluid are symbolized as λ and λ_1 while $\mathbf{R_1} = (\nabla\vec{\mathbf{V}}) + (\nabla\vec{\mathbf{V}})'$ is the Rivlin-Ericksen tensor. This model is developed with the purpose of extending the Maxwell model. The retardation time parameter which appears in the Maxwell model is specifically corrected with the time derivative of the strain rate, for which it can measure the required time for the material to react to the deformation.

A steady, 2-D and laminar flow of the Jeffrey nanofluid model with uniform ambient temperature, T_∞, and concentration, C_∞, is investigated due to a horizontal circular cylinder. The cylinder is heated at the same constant temperature, T_w, and concentration, C_w, as exhibited in the flow diagram of fig. 1. The respective $\bar{x}$- and $\bar{y}$-co-ordinates are implicated throughout the surface of the cylinder from the lowest point, $\bar{x} = 0$ and vertical to it, with a and g being the radius of the circular cylinder and gravitational acceleration, respectively. The amalgamation influences of the viscous dissipation and mixed convection are also scrutinized. The governing equations (after applying the boundary-layer approximation) are obtained:

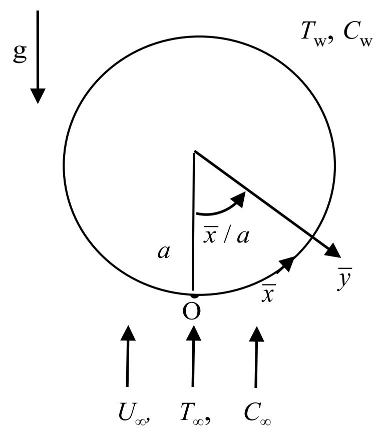

Figure 1. Flow diagram

$$\frac{\partial \bar{u}}{\partial \bar{x}} + \frac{\partial \bar{v}}{\partial \bar{y}} = 0 \tag{1}$$

$$\bar{u}\frac{\partial \bar{u}}{\partial \bar{x}}+\bar{v}\frac{\partial \bar{u}}{\partial \bar{y}}=\bar{u}_e\frac{d\bar{u}_e}{d\bar{x}}+\frac{\nu}{1+\lambda}\left[\frac{\partial^2 \bar{u}}{\partial \bar{y}^2}+\lambda_1\left(\bar{u}\frac{\partial^3 \bar{u}}{\partial \bar{x}\partial \bar{y}^2}+\bar{v}\frac{\partial^3 \bar{u}}{\partial \bar{y}^3}-\frac{\partial \bar{u}}{\partial \bar{x}}\frac{\partial^2 \bar{u}}{\partial \bar{y}^2}+\frac{\partial \bar{u}}{\partial \bar{y}}\frac{\partial^2 \bar{u}}{\partial \bar{x}\partial \bar{y}}\right)\right]+$$
$$+\mathrm{g}\beta_T(T-T_\infty)\sin\frac{\bar{x}}{a}+\mathrm{g}\beta_C(C-C_\infty)\sin\frac{\bar{x}}{a} \tag{2}$$

$$\bar{u}\frac{\partial T}{\partial \bar{x}}+\bar{v}\frac{\partial T}{\partial \bar{y}}=\alpha\frac{\partial^2 T}{\partial \bar{y}^2}+\frac{\nu}{C_p(1+\lambda)}\left[\left(\frac{\partial \bar{u}}{\partial \bar{y}}\right)^2+\lambda_1\left(\bar{u}\frac{\partial \bar{u}}{\partial \bar{y}}\frac{\partial^2 \bar{u}}{\partial \bar{x}\partial \bar{y}}+\bar{v}\frac{\partial \bar{u}}{\partial \bar{y}}\frac{\partial^2 \bar{u}}{\partial \bar{y}^2}\right)\right]+$$
$$+\tau\left[D_B\frac{\partial C}{\partial \bar{y}}\frac{\partial T}{\partial \bar{y}}+\frac{D_T}{T_\infty}\left(\frac{\partial T}{\partial \bar{y}}\right)^2\right] \tag{3}$$

$$\bar{u}\frac{\partial C}{\partial \bar{x}}+\bar{v}\frac{\partial C}{\partial \bar{y}}=D_B\frac{\partial^2 C}{\partial \bar{y}^2}+\frac{D_T}{T_\infty}\frac{\partial^2 T}{\partial \bar{y}^2} \tag{4}$$

In the previous equations, the ratio of heat capacity of the nanoparticle to the fluid and the velocity outside the boundary-layer are denoted as $\tau=(\rho c)_p/(\rho c)_\mathrm{f}$ and $\bar{u}_e(x)=U_\infty\sin(\bar{x}/a)$, respectively, whereas the velocity components along the $\bar{x}$- and $\bar{y}$-co-ordinates are symbolized as $\bar{u}$ and $\bar{v}$, respectively. Besides, the respective ratio of relaxation to retardation times, relaxation time, thermal expansion, concentration expansion, thermal diffusivity, kinematic viscosity, fluid density, local concentration, specific heat capacity at a constant pressure, local temperature, Brownian diffusion coefficient, and thermophoretic diffusion coefficient are indicated as λ, λ_1, β_T, β_C, α, ν, ρ, C, C_p, T, D_B, and D_T. Equations (1)-(4) are subjected to the following boundary conditions:

$$\begin{gathered}\bar{u}(\bar{x},0)=0,\quad \bar{v}(\bar{x},0)=0,\quad T(\bar{x},0)=T_\mathrm{w},\quad C(\bar{x},0)=C_\mathrm{w}\ \text{at}\ \bar{y}=0\\ \bar{u}(\bar{x},\infty)\to\bar{u}_e,\quad \bar{v}(\bar{x},\infty)\to 0,\quad T(\bar{x},\infty)\to T_\infty,\quad C(\bar{x},\infty)\to C_\infty\ \text{as}\ \bar{y}\to\infty\end{gathered} \tag{5}$$

The previous mathematical model can be furthered non-dimensionless using the subsequent variables:

$$\begin{gathered}x=\frac{\bar{x}}{a},\ y=\frac{\mathrm{Re}^{1/2}\,\bar{y}}{a},\ u=\frac{\bar{u}}{U_\infty},\ v=\frac{\mathrm{Re}^{1/2}\,\bar{v}}{U_\infty},\ u_e(x)=\frac{\bar{u}_e(x)}{U_\infty}\\ \theta(\eta)=\frac{T-T_\infty}{T_\mathrm{w}-T_\infty},\ \phi(\eta)=\frac{C-C_\infty}{C_\mathrm{w}-C_\infty}\end{gathered} \tag{6}$$

Using eq. (6), and eqs. (1)-(5) yield:

$$\frac{\partial u}{\partial x}+\frac{\partial v}{\partial y}=0 \tag{7}$$

$$\begin{gathered}u\frac{\partial u}{\partial x}+v\frac{\partial u}{\partial y}=u_e\frac{\mathrm{d}u_e}{\mathrm{d}x}+\frac{1}{1+\lambda}\left[\frac{\partial^2 u}{\partial y^2}+\lambda_2\left(u\frac{\partial^3 u}{\partial x\partial y^2}-\frac{\partial u}{\partial x}\frac{\partial^2 u}{\partial y^2}+v\frac{\partial^3 u}{\partial y^3}+\frac{\partial u}{\partial y}\frac{\partial^2 u}{\partial x\partial y}\right)\right]+\\ +\gamma\left[\theta+N\phi\right]\sin x\end{gathered} \tag{8}$$

$$u\frac{\partial\theta}{\partial x}+v\frac{\partial\theta}{\partial y}=\frac{1}{\Pr}\frac{\partial^2\theta}{\partial y^2}+Nb\frac{\partial\phi}{\partial y}\frac{\partial\theta}{\partial y}+Nt\left(\frac{\partial\theta}{\partial y}\right)^2+$$
$$+\frac{\mathrm{Ec}}{1+\lambda}\left[\left(\frac{\partial u}{\partial y}\right)^2+\lambda_2\left(u\frac{\partial u}{\partial y}\frac{\partial^2 u}{\partial x\partial y}+v\frac{\partial u}{\partial y}\frac{\partial^2 u}{\partial y^2}\right)\right] \tag{9}$$

$$u\frac{\partial\phi}{\partial x}+v\frac{\partial\phi}{\partial y}=\frac{1}{\mathrm{Le}\Pr}\left(\frac{\partial^2\phi}{\partial y^2}+\frac{Nt}{Nb}\frac{\partial^2\theta}{\partial y^2}\right) \tag{10}$$

$$\begin{gathered}u(x,0)=0,\quad v(x,0)=0,\quad \theta(x,0)=1,\quad \phi(x,0)=1 \quad \text{at} \quad y=0\\ u(x,\infty)\to u_e,\quad v(x,\infty)\to 0,\quad \theta(x,\infty)\to 0,\quad \phi(x,\infty)\to 0 \quad \text{as} \quad y\to\infty\end{gathered} \tag{11}$$

In consequence of the previous equations, we let Pr, λ_2, Ec, γ, Gr, Re, N, Nb, Le and Nt be the Prandtl number, Deborah number, Eckert number, mixed convection parameter, Grashof number, Reynolds number, concentration buoyancy parameter, Brownian motion parameter, Lewis number, and thermophoresis diffusion parameter, which can be expressed:

$$\Pr=\frac{\nu}{\alpha},\ \lambda_2=\frac{\lambda_1 U_\infty}{a},\ \mathrm{Ec}=\frac{U_\infty{}^2}{C_p\left(T_\mathrm{w}-T_\infty\right)},\ \gamma=\frac{\mathrm{Gr}}{\mathrm{Re}_x^2},\ \mathrm{Gr}=\frac{a^3 g\beta_T\left(T_\mathrm{w}-T_\infty\right)}{\nu^2},\ \mathrm{Re}=\frac{U_\infty a}{\nu}$$
$$N=\frac{\beta_C\left(C_\mathrm{w}-C_\infty\right)}{\beta_T\left(T_\mathrm{w}-T_\infty\right)},\ Nb=\frac{\tau D_B(C_\mathrm{w}-C_\infty)}{\nu},\ \mathrm{Le}=\frac{\alpha}{D_B},\ Nt=\frac{\tau D_T(T_\mathrm{w}-T_\infty)}{\nu T_\infty}$$

Next, we look for these variables to solve eqs. (7)-(11): $\psi=xf(x,y)$, $\theta=\theta(x,y)$ and $\phi=\phi(x,y)$, in which the stream function, ψ is represented by $u=\partial\psi/\partial y$ and $v=-\partial\psi/\partial x$. Now, the satisfaction of eq. (7) is automatically achieved and the resulting PDE together with the related boundary conditions are:

$$\frac{1}{1+\lambda}f'''-\left(f'\right)^2+ff''+\frac{\sin x}{x}\left[\gamma\left(\theta+N\phi\right)+\cos x\right]+\frac{\lambda_2}{1+\lambda}\left[\left(f''\right)^2-ff^{(iv)}\right]=$$
$$=x\left[f'\frac{\partial f'}{\partial x}-f''\frac{\partial f}{\partial x}+\frac{\lambda_2}{1+\lambda}\left(f'''\frac{\partial f'}{\partial x}+f^{(iv)}\frac{\partial f}{\partial x}-f''\frac{\partial f''}{\partial x}-f'\frac{\partial f'''}{\partial x}\right)\right] \tag{12}$$

$$\frac{1}{\Pr}\theta''+f\theta'+Nb\theta'\phi'+Nt\left(\theta'\right)^2=$$
$$=x\left(f'\frac{\partial\theta}{\partial x}-\theta'\frac{\partial f}{\partial x}-x\frac{\mathrm{Ec}}{(1+\lambda)}\left\{\left(f''\right)^2+\lambda_2\left[xff''\frac{\partial f''}{\partial x}+f'\left(f''\right)^2-xf''f'''\frac{\partial f}{\partial x}-ff''f'''\right]\right\}\right) \tag{13}$$

$$\phi''+\mathrm{Le}\Pr f\phi'+\frac{Nt}{Nb}\theta''=x\mathrm{Le}\Pr\left[f'\frac{\partial\phi}{\partial x}-\phi'\frac{\partial f}{\partial x}\right] \tag{14}$$

$$\begin{gathered}f(x,0)=0,\ f'(x,0)=0,\ \theta(x,0)=1,\ \phi(x,0)=1 \ \text{at} \ y=0\\ f'(x,\infty)\to\frac{\sin x}{x},\ f''(x,\infty)\to 0,\ \theta(x,\infty)\to 0,\ \phi(x,\infty)\to 0 \ \text{as} \ y\to\infty\end{gathered} \tag{15}$$

Note that primes infer the differentiation with respect to the variable y. Also, we found that eqs. (12)-(15) can be reduced to the mixed convection Newtonian fluid as reported by Mohamed *et al.* [22], provided the absence of the Jeffrey fluid $(\lambda = \lambda_2 = 0)$ and nanofluid $(Nt = Nb = \mathrm{Le} = N = 0)$ parameters. At the vicinity of the lower stagnation point ($x \approx 0$), the preceding equations, eqs. (12)-(15), give rise to the succeeding ODE:

$$\frac{1}{1+\lambda} f''' + ff'' - (f')^2 + 1 + \gamma(\theta + N\phi) + \frac{\lambda_2}{1+\lambda}\left[(f'')^2 - ff^{(iv)}\right] = 0 \tag{16}$$

$$\frac{1}{\mathrm{Pr}}\theta'' + f\theta' + Nb\theta'\phi' + Nt(\theta')^2 = 0 \tag{17}$$

$$\phi'' + \mathrm{Le}\,\mathrm{Pr}\, f\phi' + \frac{Nt}{Nb}\theta'' = 0 \tag{18}$$

$$\begin{gathered} f(0) = 0,\ f'(0) = 0,\ \theta(0) = 1,\ \phi(0) = 1 \\ f'(\infty) \to 1,\ f''(\infty) \to 0,\ \theta(\infty) \to 0,\ \phi(\infty) \to 0 \end{gathered} \tag{19}$$

The non-appearance of Eckert number parameter in eq. (17) clearly signifies that the profiles for velocity, temperature and concentration are no longer being influenced by Eckert at the stagnation point of the cylinder. Further, the reduced Nusselt and Sherwood numbers are now given:

$$\mathrm{Nu}_x \mathrm{Re}_x^{-1/2} = -\theta'(x,0) \quad \text{and} \quad \mathrm{Sh}_x \mathrm{Re}_x^{-1/2} = -\phi'(x,0) \tag{20}$$

Results and discussion

Figures 2-15 and tabs. 1-3 illustrate the comprehensive numerical results for eight thermophysical and body force control parameters such as λ, λ_2, γ, Nt, Nb, Le, and Ec. These results are accomplished by solving the preceding highly non-linear PDE *i. e.* eqs. (12)-(14) with boundary conditions eq. (15) via the Keller-box method [23]. The appropriate step size of $\Delta x = 0.01$ and $\Delta y = 0.01$ and the thickness of boundary-layer of $y_\infty = 6$ are implemented to ensure the solutions reach the asymptotic values acceptably. All parameters are customized as follows, if not declared elsewhere: $\lambda = \lambda_2 = \gamma = \mathrm{Ec} = 0.1$, $N = Nb = Nt = 0.3$, $\mathrm{Le} = 10$ and $\mathrm{Pr} = 1$. Furthermore, authentication for the results is acquired by way of comparisons, as accessible in tab. 1. The current numerical values are compared with those of several existing publications and the values appear to be very much in line. Such positive outcome brings in a supreme conviction in all results as disclosed later.

Table 1. Comparative results for various values of γ when $\mathrm{Pr} = 1$, $Nb = Nt = N = \lambda = \mathrm{Ec} = 0$ and $\lambda_2 \to 0$ (very small)

	$-\theta'(0)$			
γ	[15]	[16]	[19]	Present
–1.0	0.5067	0.5080	0.5068	0.5067
–0.5	0.5420	0.5430	0.5421	0.5421
0.0	0.5705	0.5710	0.5706	0.5705
0.88	0.6096	0.6112	0.6111	0.6108
0.89	0.6110	0.6116	0.6114	0.6112
2.0	0.6497	0.6518	0.6518	0.6515
5.0	0.7315	0.7320	0.7319	0.7315

Figures 2 and 3 exemplify the impacts of parameters λ and λ_2 on the velocity field. In fig. 2, the velocity field is accelerated due to parameter λ. The reason is that increasing λ indicates the enhancement of relaxation time that simultaneously weakens the retardation time. As such, the velocity field, together with the thickness of momentum boundary-layer, display improvement. However, parameter λ_2 acts as opposed to that of λ, where the fluid-flow is lessened with increasing values of λ_2, fig. 3. Physically, as λ_2 escalates, the material tends to be gradually affected by the viscoelasticity that exhibits both viscous and elastic behaviors. Flow with a lower λ_2 specifies that the fluid is in a viscous state, hence leading to the rapid convergent of the velocity field. Meanwhile, as for high λ_2, the fluid is relatively elastic (solid-like manner), thus the presence of viscosity and elasticity slows down the flow of fluid.

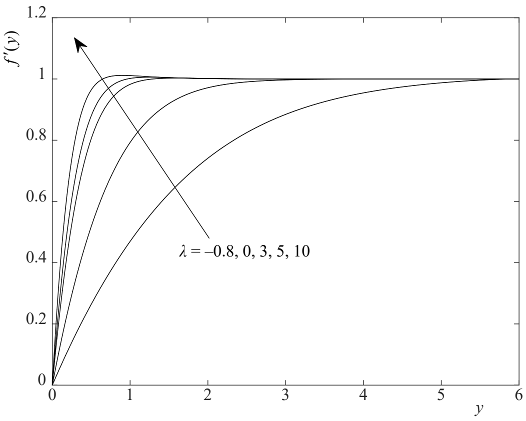

Figure 2. The $f'(y)$ *vs.* y for sundry values of λ

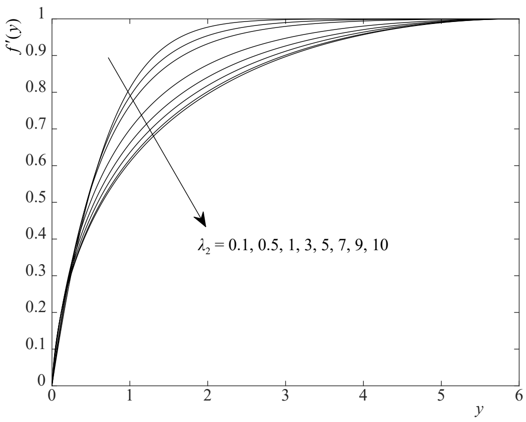

Figure 3. The $f'(y)$ *vs.* y for sundry values of λ_2

Figures 4 and 5 divulge that the parameter γ has an increasing impact on the velocity field and a decreasing impact on the temperature field. Parameter γ is in actual fact an amalgamation of viscosity and buoyancy forces, where γ is inversely proportional to the viscous forces. Here, an increase in γ entails the enhancement of buoyancy force effect, which concurrently reinforces the favorable pressure gradient and subsequently, accelerating the motion of the fluid while reducing the temperature.

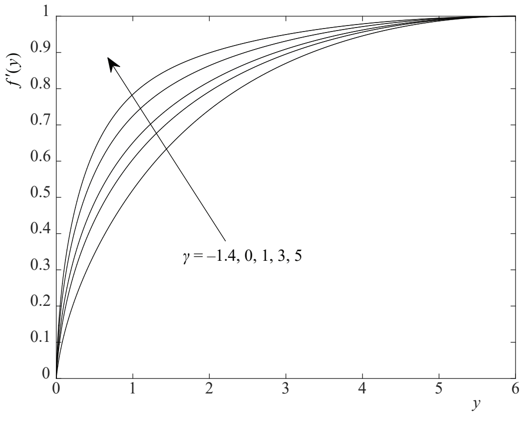

Figure 4. The $f'(y)$ *vs.* y for sundry values of γ

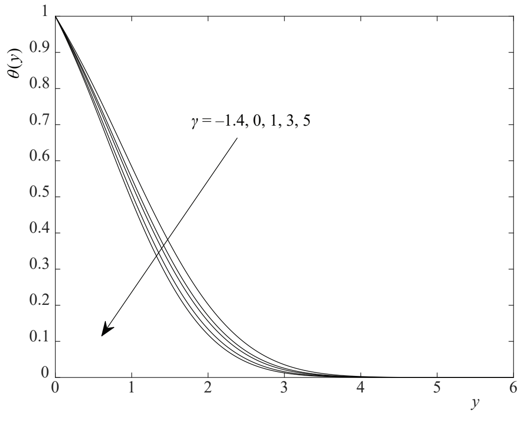

Figure 5. The $\theta(y)$ *vs.* y for sundry values of γ

In fig. 6, a significant growth of the temperature profile is observed along with the increment of *Nb*. Physically, *Nb* is defined as the suspended particles that move randomly in the fluid, which is predominantly instigated by collision among fluid molecules or quick atoms. This collision tends to heighten as *Nb* increases and consequently, intensify the temperature field. Likewise, fig. 7 depicts a considerable development of the temperature field with the increment of *Nt*. The augmentation of *Nt* generates a stronger thermophoretic force that permits a broad passage of nanoparticles from the hot surface of the cylinder. Accordingly, a particle free-layer is formed in the vicinity of the surface, whereas the spreading of nanoparticles is reinforced on the outside.

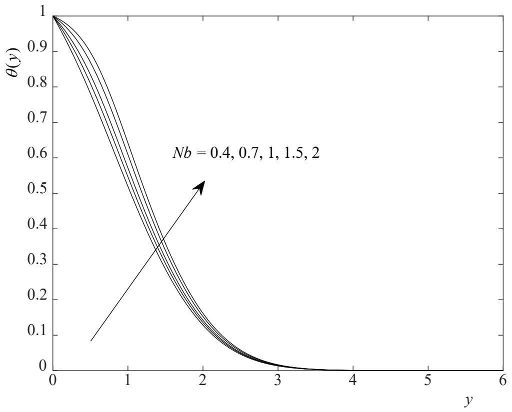

Figure 6. The $\theta(y)$ *vs.* *y* for sundry values of *Nb*

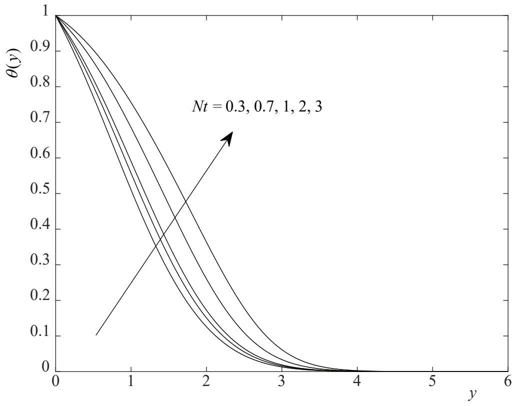

Figure 7. The $\theta(y)$ *vs.* *y* for sundry values of *Nt*

Figures 8 and 9 demonstrate the results for the concentration field against Le and *Nb.* As displayed in fig. 8, the concentration field and its related boundary-layer thickness are intensely degenerated when Lewis number values intensify. From the definition, $\text{Le} = \alpha/D_B$, where the Brownian diffusion coefficient, D_B, has control over Lewis number. It follows that Lewis number is toughened for smaller D_B but weakened for larger D_B. Such smaller D_B is then linked with the lower concentration field. Likewise, a slight decay of concentration field is attributable to the increasing *Nb*, as exposed in fig. 9. This is physically caused by the Brownian impact in which nanoparticles are transported randomly under diverse velocities.

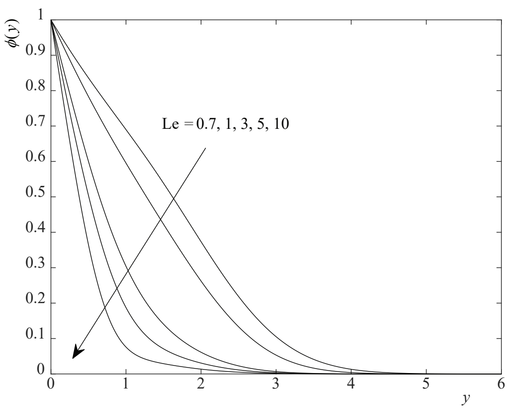

Figure 8. The $\phi(y)$ *vs.* y for sundry values of Le

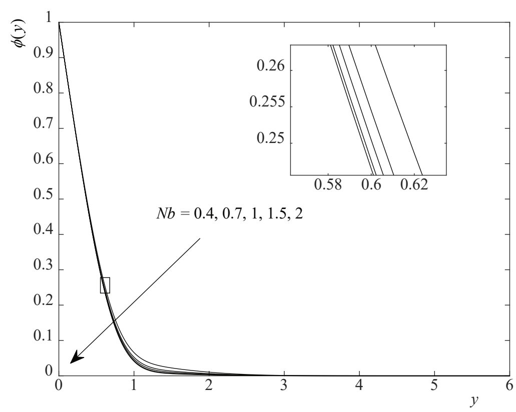

Figure 9. The $\phi(y)$ *vs.* y for sundry values of *Nb*

Results of the Nusselt number, $\mathrm{Nu}_x\mathrm{Re}_x^{-1/2}$, and Sherwood number, $\mathrm{Sh}_x\mathrm{Re}_x^{-1/2}$, are accessible through figs. 10-15 for some dimensionless parameters of λ_2, *Nb*, and Ec. Figures 10 and 11 present the outcome of parameter λ_2 on the $\mathrm{Nu}_x\mathrm{Re}_x^{-1/2}$ and $\mathrm{Sh}_x\mathrm{Re}_x^{-1/2}$. With greater viscoelasticity property, the $\mathrm{Nu}_x\mathrm{Re}_x^{-1/2}$ is moderately reduced while the $\mathrm{Sh}_x\mathrm{Re}_x^{-1/2}$ is alternatively declined and then enhanced. It is found from numerical computation that the acceptable solution for λ_2 is in the range of $0 \le \lambda_2 \le 30$. Interestingly, the boundary-layer separation can be suppressed in the range of $0° \le x \le 120°$, for which the earliest separation happens when $\lambda_2 = 0.1$, and then it delays continuously as λ_2 increases. Specifically, the separation point for $\lambda_2 = 0.1,\ 0.5,\ 1,\ 3,\ 5,\ 7,\ 9,\ 10$ happens at:

$$x = 72.19°,\ 73.34°,\ 74.48°,\ 83.65°,\ 95.11°,\ 109.43°,\ 120°,\ 120°$$

with their respective critical values of:

$$\mathrm{Nu}_x\mathrm{Re}_x^{-1/2} = 0.2801,\ 0.2769,\ 0.2741,\ 0.2564,\ 0.2382,\ 0.2178,\ 0.1925,\ 0.1808$$

and

$$\mathrm{Sh}_x\mathrm{Re}_x^{-1/2} = 1.0788,\ 1.0751,\ 1.0758,\ 1.0473,\ 1.0118,\ 0.9830,\ 1.0108,\ 1.0504$$

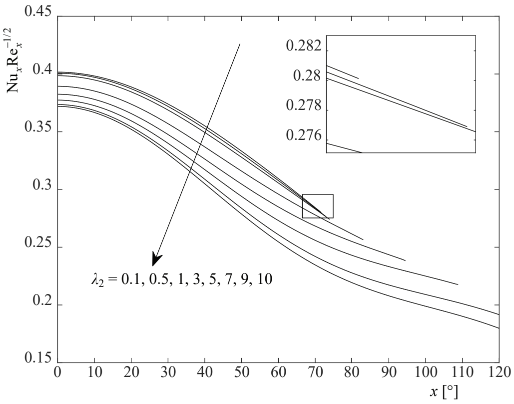

Figure 10. The $\mathrm{Nu}_x\mathrm{Re}_x^{-1/2}$ *vs.* *x* for sundry values of λ_2

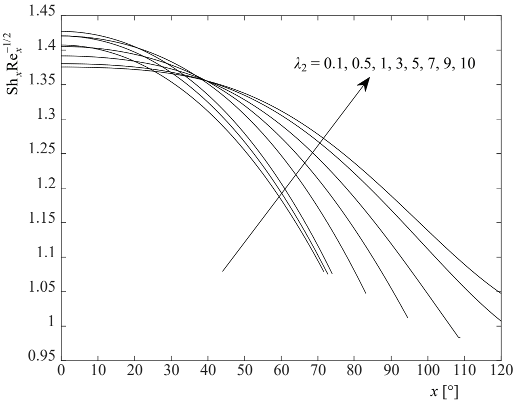

Figure 11: The $\mathrm{Sh}_x\mathrm{Re}_x^{-1/2}$ *vs.* *x* for sundry values of λ_2

In fig. 12, a very strong depletion of $\mathrm{Nu}_x\mathrm{Re}_x^{-1/2}$ is observed with the increasing *Nb* values. This consequence is forecasted since it complies with the thermal boundary-layer augmentation imposed by dissimilar *Nb* values in fig. 6. Similarly, the $\mathrm{Sh}_x\mathrm{Re}_x^{-1/2}$ is a declining function of *Nb*, which suggests the ongoing deprivation of nanoparticles transfer rate, fig. 13. The effect of parameter Eckert number is displayed in figs. 14 and 15. With the increment in Eckert number, a notable decrement in the $\mathrm{Nu}_x\mathrm{Re}_x^{-1/2}$ is revealed, but the $\mathrm{Sh}_x\mathrm{Re}_x^{-1/2}$ acts contrarily. It is noticed that fig. 14 gives negative values of the $\mathrm{Nu}_x\mathrm{Re}_x^{-1/2}$, that reflect the reversal of heat flow [24]. This circumstance relates with the dissipation generated by the shear stress in the fluid at the cylinder surface, where the cylinder is understood to not cool anymore, but continuously takes up heat regardless of its higher wall temperature than the ambient temperature. Such *self-heating temperature* outcome is therefore expected to induce the drop in heat transfer. Furthermore, it is also identified that the graphs for velocity, temperature and concentration fields are unique because of termination of Eckert number at the lower stagnation point. Therefore, these graphs are not put forward for further discussion. Also, for increasing *Nb* and Ec values, the numerical computation discloses that figs. 12-15 undergo singularity for $x > 71.05°$.

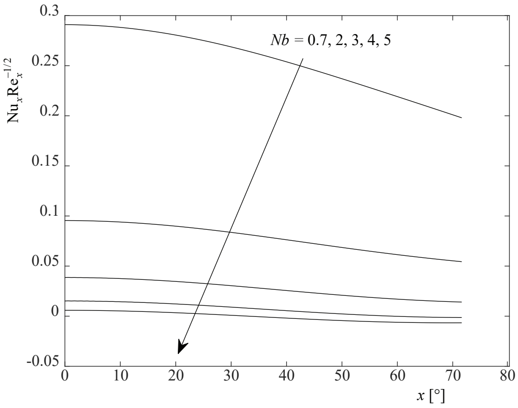

Figure 12. The $Nu_x Re_x^{-1/2}$ *vs.* x for sundry values of *Nb*

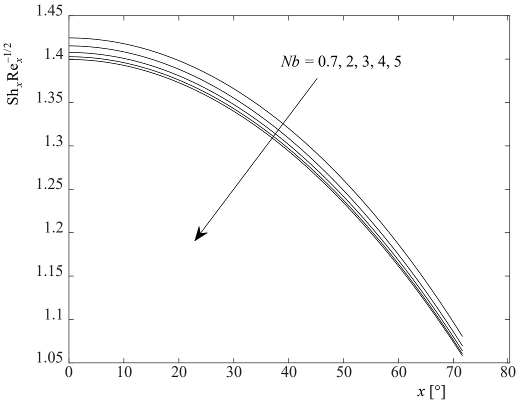

Figure 13. The $Sh_x Re_x^{-1/2}$ *vs.* x for sundry values of *Nb*

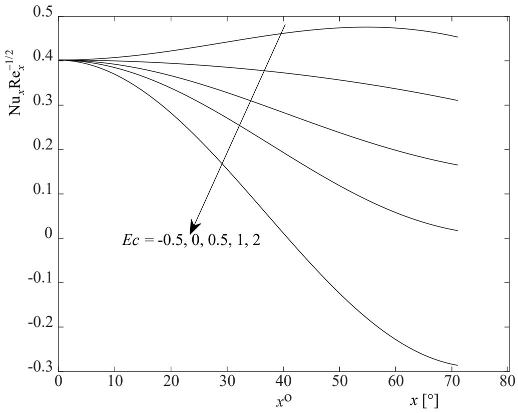

Figure 14. The $Nu_x Re_x^{-1/2}$ *vs.* x for sundry values of Ec

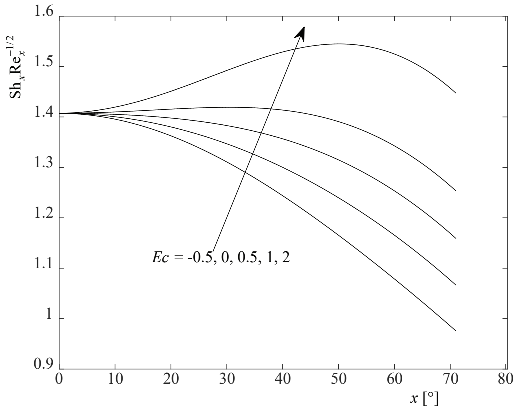

Figure 15. The $Sh_x Re_x^{-1/2}$ *vs.* x for sundry values of Ec

Tables 2 and 3 tabulate the numerical results of the $Nu_x Re_x^{-1/2}$ and the $Sh_x Re_x^{-1/2}$ for diverse values of γ with respect to the varied positions of x. It is detected that when γ increases, the $Nu_x Re_x^{-1/2}$ rises to a maximum value and then declines to a finite value. Also, γ has an increasing impact on the $Sh_x Re_x^{-1/2}$. These circumstances may be linked to figs. 4 and 5, where γ is liable to the escalation of fluid-flow and convection cooling effect. It is worth to highlight here that these behaviors are also in line with those reported by Merkin [15], Nazar *et al.* [16], and Rashad *et al.* [19]. As depicted from these tables, the separation of boundary-layer occurs for both positive (assisting flow) and negative (opposing flow) values of γ. For appropriately large positive values of $\gamma (> 0)$, the cylinder is heated and the boundary-layer separation appears to postpone within the range of $0 \le x \le 120°$. Meanwhile, for appropriately small negative values of $\gamma (< 0)$, the cylinder is cooled and the separation point is conveyed near to the lower stagnation point. Here, there exists a point where the boundary-layer solution becomes impossible. The reason is that, free convection begins at the top stagnation point of the cylinder

($x = \pi$) and there exists a point in which the upwards stream flow does not have the ability to defeat the fluid tendency near the cylinder to passage underneath due to the buoyancy force effect. This situation is considered as unstable, hence either a boundary-layer transpires on the surface of the cylinder is still an unanswered question [15, 25].

Table 2. Numerical results of $Nu_x Re_x^{-1/2}$ for diverse values of γ at different positions of x

$x \backslash \gamma$ [°]	–1.4	0	1	2	3	4	5
0	0.2925	0.3974	0.4340	0.4620	0.4851	0.5049	0.5224
10		0.3942	0.4302	0.4573	0.4792	0.4978	0.5140
20		0.3846	0.4187	0.4428	0.4614	0.4763	0.4885
30		0.3704	0.4017	0.4216	0.4352	0.4445	0.4508
40		0.3510	0.3790	0.3931	0.3998	0.4015	0.3995
50		0.3297	0.3547	0.3627	0.3619	0.3551	0.3439
60		0.3049	0.3279	0.3294	0.3200	0.3036	0.2818
70			0.3030	0.2987	0.2815	0.2559	0.2240
80			0.2795	0.2705	0.2461	0.2119	0.1703
90			0.2566	0.2443	0.2137	0.1716	0.1210
100				0.2224	0.1873	0.1393	0.0816
110					0.1682	0.1166	0.0545
120						1.0216	0.0382

Table 3. Numerical results of $Sh_x Re_x^{-1/2}$ for diverse values of γ at different positions of x

$x \backslash \gamma$ [°]	–1.4	0	1	2	3	4	5
0	0.8660	1.3878	1.5541	1.6781	1.7788	1.8643	1.9391
10		1.3817	1.5502	1.6757	1.7776	1.8642	1.9402
20		1.3628	1.5380	1.6679	1.7736	1.8638	1.9433
30		1.3325	1.5182	1.6550	1.7664	1.8620	1.9468
40		1.2863	1.4880	1.6344	1.7539	1.8571	1.9493
50		1.2281	1.4500	1.6076	1.7362	1.8478	1.9483
60		1.1497	1.3989	1.5704	1.7096	1.8310	1.9411
70			1.3404	1.5262	1.6760	1.8069	1.9262
80			1.2722	1.4731	1.6334	1.7734	1.9016
90			1.1901	1.4076	1.5781	1.7268	1.8632
100				1.3334	1.5127	1.6683	1.8112
110					1.4424	1.6023	1.7490
120						1.5310	1.6790

Conclusions

This paper presents the influence of viscous dissipation on the mixed convection boundary-layer flow induced by a horizontal circular cylinder filled in a Jeffrey nanofluid. In general, this study has exposed the effects of parameters λ, λ_2, γ, Le, Nb, Nt, and Ec upon velocity, temperature and concentration fields as well as the Nusselt and Sherwood numbers. The following conclusions can be deduced from this study:

- The velocity field rises due to parameters λ and γ, but declines because of parameter λ_2.
- The increment in temperature field is attributable to parameters Nt and Nb, but deteriorates as a result of parameter γ.

- The concentration field diminishes as a consequence of parameters Le and *Nb*.
- For the dissimilar values of Eckert number, the velocity, temperature and concentration fields pronounce no effect as Eckert number discontinues at $x = 0$.
- The Nusselt number degenerates with the rising values of λ_2, Nb, and Ec.
- The Sherwood number is the growing function of parameters λ_2 and Ec, and is the declining function of parameter *Nb*.
- The separation of boundary-layer occurs for both positive (cooled cylinder) and negative (heated cylinder) values of γ, and that separation can be surpressed within $0° \le x \le 120°$.
- Increasing the values of λ_2 have delayed the boundary-layer separation up to $x = 120°$, while parameters *Nb* and Ec undergo singularity for $x > 71.05°$.

Acknowledgment

This work is supported by University Malaysia Pahang (UMP) through grants (RDU170358 and PGRS1703100). The authors are very much thankful to the provisions given as well as the valuable comments and suggestions from the reviewers.

Nomenclature

a	–	radius of the cylinder
c	–	specific heat capacity of the nanoparticle material
C	–	concentration
C_p	–	specific heat capacity at constant pressure, [Jkg^{-1}K^{-1}]
C_w	–	concentration at the surface
C_∞	–	ambient concentration
D_B	–	Brownian diffusion coefficient, [m^{2}s^{-1}]
D_T	–	thermophoretic diffusion coefficient, [m^{2}s^{-1}]
Ec	–	Eckert number
f	–	dimensionless stream function, [ms^{-1}]
g	–	gravitational acceleration, [ms^{-2}]
Gr	–	Grashof number
$\mathbf{I}$	–	identity tensor
Le	–	Lewis numbers
N	–	concentration buoyancy parameter
Nb	–	Brownian motion parameter
Nt	–	thermophoresis parameter
$\mathrm{Nu}_x\mathrm{Re}_x^{-1/2}$	–	reduced Nusselt number
p	–	pressure, [Pa]
Pr	–	Prandtl number
$\mathbf{R_1}$	–	Rivlin-Erickson tensor
Re	–	Reynolds number
$\mathbf{S}$	–	extra stress tensor
$\mathrm{Sh}_x\mathrm{Re}_x^{-1/2}$	–	reduced Sherwood number
t	–	time
T	–	fluid temperature, [K]
T_w	–	wall temperature, [K]
T_∞	–	ambient temperature, [K]
$\overline{u}$, u	–	velocity components along the x-direction, [ms^{-1}]
$\overline{u}_e$, u_e	–	velocity outside the boundary-layer
U_∞	–	free stream velocity
$\vec{\mathbf{V}}$	–	velocity vector
$\overline{v}$, v	–	velocity components along the y-direction, [ms^{-1}]
$\overline{x}$, x	–	co-ordinates along the surface
$\overline{y}$, y	–	co-ordinates normal to the surface
y_∞	–	boundary-layer thickness

Greek Symbols

α	–	thermal diffusivity, [m^{2}s^{-1}]
β_C	–	concentration expansion coefficient
β_T	–	thermal expansion coefficient, [K^{-1}]
ρ	–	fluid density
λ	–	ratio of relaxation to retardation times
λ_1	–	retardation time
λ_2	–	Deborah number
θ	–	dimensionless temperature
ϕ	–	dimensionless nanoparticle concentration
μ	–	dynamic viscosity, [kgm^{-1}s^{-1}]
ν	–	kinematic viscosity, [m^{2}s^{-1}]
γ	–	mixed convection parameter
τ	–	ratio of heat capacity of nanoparticle to the base fluid
$\boldsymbol{\tau}$	–	Cauchy stress tensor, [kgm^{-1}s^{-2}]
ψ	–	stream function
∇	–	vector divergence

Subscripts

f	–	fluid
w	–	condition at the surface of the cylinder

Superscripts

‘ – differentiation with respect to y
p – nanoparticle material
∞ – condition at the free stream
– – dimensional variables

References

[1] Ramzan, M., *et al.*, Double Stratified Radiative Jeffery Magneto Nanofluid Flow along an Inclined Stretched Cylinder with Chemical Reaction and Slip Condition, *The European Physical Journal Plus*, *132* (2017), 11, 456

[2] Eastman, J., *et al.* Enhanced Thermal Conductivity through the Development of Nanofluids, *Proceedings*, Symposium V – Nanophase and Nanocomposite Materials II, Boston, Mass., USA, 1996, Vol. 457

[3] Eastman, J. A., *et al.*, Anomalously Increased Effective Thermal Conductivities of Ethylene Glycol-based Nanofluids Containing Copper Nanoparticles, *Applied Physics Letters*, *78* (2001), 6, pp. 718-720

[4] Choi, S., *et al.*, Anomalous Thermal Conductivity Enhancement in Nanotube Suspensions, *Applied Physics Letters*, *79* (2001), 14, pp. 2252-2254

[5] Kuznetsov, A., Nield, D., Natural Convective Boundary-Layer Flow of a Nanofluid Past a Vertical Plate, *International Journal of Thermal Sciences*, *49* (2010), 2, pp. 243-247

[6] Khan, W., Pop, I., Boundary-Layer Flow of a Nanofluid Past a Stretching Sheet, *International Journal of Heat and Mass Transfer*, *53* (2010), 11, pp. 2477-2483

[7] Sheikholeslami, M., *et al.*, Combined Thermophoresis and Brownian Motion Effects on Nanofluid Free Convection Heat Transfer in an L-Shaped Enclosure, *Chinese Journal of Physics*, *55* (2017), 6, pp. 2356-2370

[8] Khan, U., *et al.*, Nonlinear Radiation Effects on MHD Flow of Nanofluid over a Nonlinearly Stretching/Shrinking Wedge, *Neural Computing and Applications*, *28* (2017), 8, pp. 2041-2050

[9] Kandasamy, R., *et al.*, Thermal and Solutal Stratification on MHD Nanofluid Flow over a Porous Vertical Plate, *Alexandria Engineering Journal*, *57* (2018), 1, pp. 121-130

[10] Shehzad, S., *et al.*, MHD Flow of Jeffrey Nanofluid with Convective Boundary Conditions, *Journal of the Brazilian Society of Mechanical Sciences and Engineering*, *37* (2015), 3, pp. 873-883

[11] Dalir, N., *et al.*, Entropy Analysis for Magnetohydrodynamic Flow and Heat Transfer of a Jeffrey Nanofluid over a Stretching Sheet, *Energy*, *79* (2015), Jan., pp. 351-362

[12] Abbasi, F., *et al.*, Mixed Convection Flow of Jeffrey Nanofluid with Thermal Radiation and Double Stratification, *Journal of Hydrodynamics, Ser. B*, *28* (2016), 5, pp. 840-849

[13] Hayat, T., *et al.*, A Revised Model for Jeffrey Nanofluid Subject to Convective Condition and Heat Generation/Absorption, *PloS One*, *12* (2017), 2, e0172518

[14] Sharma, K., Gupta, S., Viscous Dissipation and Thermal Radiation Effects in MHD Flow of Jeffrey Nanofluid through Impermeable Surface with Heat Generation/Absorption, *Nonlinear Engineering*, *6* (2017), 2, pp. 153-166

[15] Merkin, J., Mixed Convection from a Horizontal Circular Cylinder, *International Journal of Heat and Mass Transfer*, *20* (1977), 1, pp. 73-77

[16] Nazar, R., *et al.*, Mixed Convection Boundary-Layer Flow from a Horizontal Circular Cylinder in Micropolar Fluids: Case of Constant Wall Temperature, *International Journal of Numerical Methods for Heat & Fluid Flow*, *13* (2003), 1, pp. 86-109

[17] Anwar, I., *et al.*, Mixed Convection Boundary Layer Flow of a Viscoelastic Fluid over a Horizontal Circular Cylinder, *International Journal of Non-Linear Mechanics*, *43* (2008), 9, pp. 814-821

[18] Salleh, M. Z., *et al.*, Mixed Convection Boundary Layer Flow over a Horizontal Circular Cylinder with Newtonian Heating, *Heat and Mass Transfer*, *46* (2010), 11-12, pp. 1411-1418

[19] Rashad, A., *et al.*, Mixed Convection Boundary-Layer Flow past a Horizontal Circular Cylinder embedded in a Porous Medium Filled with a Nanofluid under Convective Boundary Condition, *Computers & Fluids*, *86* (2013), Nov., pp. 380-388

[20] Tham, L., *et al.*, Mixed Convection Flow from a Horizontal Circular Cylinder embedded in a Porous Medium Filled by a Nanofluid: Buongiorno–Darcy Model, *International Journal of Thermal Sciences*, *84* (2014), Oct., pp. 21-33

[21] Qasim, M., Heat and Mass Transfer in a Jeffrey Fluid over a Stretching Sheet with Heat Source/Sink, *Alexandria Engineering Journal*, *52* (2013), 4, pp. 571-575

[22] Mohamed, M. K. A., *et al.*, The Viscous Dissipation Effects on The Mixed Convection Boundary Layer Flow on a Horizontal Circular Cylinder, *Jurnal Teknologi*, *78* (2016), 4-4, pp. 73-79

[23] Zokri, S. M., *et al.* Numerical Solutions on Mixed Convection Boundary Layer and Heat Transfer of Jeffrey Fluid over a Horizontal Circular Cylinder by using Keller-box Method, *Proceedings*, The National Conference for Postgraduate Research 2016, Pekan, Pahang, Malaysia, 2016, pp. 913-926

[24] Gschwendtner, M., The Eckert Number Phenomenon: Experimental Investigations on The Heat Transfer from a Moving Wall in The Case of a Rotating Cylinder, *Heat and Mass Transfer*, *40* (2004), 6-7, pp. 551-559

[25] Kasim, A. R. M., *et al.*, Constant Heat Flux Solution for Mixed Convection Boundary Layer Viscoelastic Fluid, *Heat and Mass Transfer*, *49* (2013), 2, pp. 163-171

Paper submitted: October 27, 2018
Paper revised: March 10, 2019
Paper accepted: March 19, 2019